Article

Cholesterol Alters the Orientation and Activity of the Influenza Virus M2 Amphipathic Helix in the Membrane

Published as part of The Journal of Physical Chemistry virtual special issue "Computational and Experimental Advances in Biomembranes"

Agnieszka Martyna,[▽] Basma Bahsoun,[▽] Jesper J. Madsen, Frederic St. J. S. Jackson, Matthew D. Badham, Gregory A. Voth,* and Jeremy S. Rossman*

Read Online

ACCESS | Metrics & More | Article Recommendations | SI Supporting Information

ABSTRACT: The influenza virus M2 amphipathic helix (M2AH) alters membrane curvature in a cholesterol-dependent manner, mediating viral membrane scission during influenza virus budding. Here, we have investigated the biophysical effects of cholesterol on the ability of an M2AH peptide to manipulate membrane properties. We see that the ability of the M2AH to interact with membranes and form an α-helix is independent of membrane cholesterol concentration; however, cholesterol affects the angle of the M2AH peptide within the membrane. This change in membrane orientation affects the ability of the M2AH to alter lipid order. In low-cholesterol membranes, the M2AH is inserted near the level of the lipid head groups, increasing lipid order, which may contribute to generation of the membrane curvature. As the cholesterol content increases, the M2AH insertion becomes flatter and slightly deeper in the membrane below the lipid headgroups, where the polar face can continue to interact with the headgroups while the hydrophobic face binds cholesterol. This changed orientation minimizes lipid packing defects and lipid order changes, likely reducing the generation of membrane curvature. Thus, cholesterol regulates M2 membrane scission by precisely modulating M2AH positioning within the membrane. This has implications for the understanding of many of amphipathic-helix-driven cellular budding processes that occur in specific lipid environments.
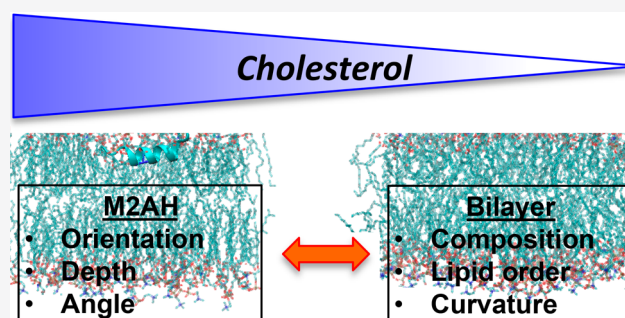
INTRODUCTION

Influenza A viruses (IAV) assemble at and bud from cholesterol- and sphingolipid-enriched lipid microdomains on the apical plasma membrane of infected cells.[1] The final step of IAV budding is membrane scission, wherein the neck of the budding virion is constricted to the point at which spontaneous fusion of the opposing membranes can occur, resulting in the release of the mature virion. The process of IAV-membrane scission is mediated by the viral M2 protein,[2] which is a 97 amino acid homotetrameric transmembrane protein that has ion channel activity during virus entry.[3−7] During virus budding, M2 is recruited to assembly sites through interactions with the viral M1 matrix and hemagglutinin (HA) proteins, which recruit M2 to the periphery of the lipid microdomains of assembling virus, placing M2 at the lipid phase boundary between the lipid ordered virus budding domain and the surrounding lipid disordered phase.[8−11] The ability of the M2 protein to mediate membrane scission is dependent on the membrane insertion of a membrane-proximal amphipathic helix (AH) domain.[2,12,13] The M2AH is 16 amino acids long and forms an α-helix upon association with the membrane.[2,14−17] Once formed, the AH contains many bulky hydrophobic residues on one face and several highly polar K/R residues on the opposite face. While these polar residues likely interact with the polar lipid headgroups, the hydrophobic face of the domain drives membrane binding.[17] The insertion of the AH domain causes membrane scission, likely by altering membrane curvature.[2,12,13] However, the M2AH also senses membrane curvature, sorting to the most highly curved region of the membrane neck, where it increases membrane order, placing the membrane neck under further strain and enhancing scission efficiency.[11,18,19]

Given that the M2 protein sorts to the sites of virus assembly early in the budding process, before membrane scission, regulatory mechanisms must be in place to prevent the early
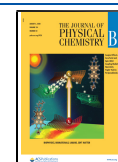
induction of membrane curvature and premature scission.[1,20] One regulatory mechanism may be the weak nature of M2AH curvature induction,[18] such that the induction is only sufficient to cause scission on a highly constricted membrane neck, ensuring scission at the appropriate spatiotemporal location. Importantly, M2AH mediation of membrane scission has been shown to be dependent on its lipid environment, specifically on the amount of surrounding membrane cholesterol.[2] When the local membrane cholesterol concentration is at 20−30 mol %, the ability of the M2AH to alter membrane curvature is reduced and membrane scission is prevented.[2] This activity is restored when the cholesterol concentration is reduced below 15%. Several reports have shown that M2 can bind cholesterol, and multiple potential binding sites have been proposed.[21] It was shown that the M2AH contains a cholesterol recognition amino acid consensus (CRAC) domain and mutation of the key Y52 residue reduced cholesterol association; however, CRAC mutations did not affect M2 targeting to lipid raft domains or virus budding.[22,23] Conversely, mutation of the M2AH palmitoylated residue C50 affected M2 raft targeting but did not reduce M2 cholesterol association, as has been shown for other palmitoylated proteins.[22,24,25] In 2016, it was predicted by solid-state NMR (ssNMR) experiments that the M2 protein binds cholesterol through an interhelical crevice on the outside of the tetrameric transmembrane domain (TMD) and through bulky hydrophobic residues on the AH including F54.[26] Further ssNMR experiments refined this model, showing that each M2 tetramer binds two cholesterol molecules through hydrophobic interactions along the TMD and through polar and aromatic interactions with F47 of the AH and F57/R61 of the neighboring AH domain.[27] These experiments suggest that both the TMD and an isolated AH domain have some capacity to interact with cholesterol through specific interactions, although the interaction is likely strongest in the context of the full-length protein. In the context of the full-length protein, association with membrane cholesterol appears to stabilize the AH and alter the orientation of the AH domain in the membrane, although the effects of this change on M2AH activity are not known.[28−30] In this study, we have sought to determine the biophysical mechanisms by which membrane cholesterol concentrations modulate M2AH activity. Given the myriad of AH domain-containing proteins that regulate a range of essential cellular processes, understanding the regulatory mechanisms of AH domains and their intricate interplay with membrane composition is of broad importance.

■ METHODS

All peptides were synthesized by Biomatik (Wilmington, DE, USA) at 98% purity, with TFA removed. Peptide sequences included N-terminal acylation, C-terminal amidation, and a C50S mutation to prevent Cys oxidation. Sequences were as follows: M2AH (47−62 of A/Udorn/72) Ac-FFKSIYRF-FEHGLKRG-Am; M2AH-F47W Ac-**W**FKSIYRF-FEHGLKRG-Am; M2AH-Y52W Ac-FFKSI**W**RF-FEHGLKRG-Am; M2AH-F54W Ac-FFKSIYR**W**-FEHGLKRG-Am. Fluorescent M2AH incorporates FITC conjugated to K60, as previously reported.[17,18] Lipids were dissolved in chloroform and include the following: cholesterol (Ch), 1-palmitoyl-2-oleoyl-*sn*-glycero-3-phospho-1-rac-glycerol (POPG), 1-palmitoyl-2-oleoyl-*sn*-glycero-3-phosphocholine (POPC), 1-palmitoyl-2-(6,7-dibromo) stearoyl-*sn*-glycero-3-phosphocholine (6,7Br-POPC), and 1-palmitoyl-2-(11,12-

dibromo) stearoyl-*sn*-glycero-3-phosphocholine (11,12Br-POPC) (Avanti Polar Lipids, Alabaster, AL, USA). Chloroform and deuterium oxide (D_2O) were obtained from Sigma−Aldrich (Dorset, U.K.).

Large Unilamellar Vesicles. Large unilamellar vesicles (LUVs) were made by extrusion. Lipid solutions containing 12.5 μmol of lipids were made using a 4:1 molar ratio of POPC:POPG and incorporating 0.5, 1, 15, or 30 mol % Ch, as previously described.[17,18] In brief, the lipid solution was dried under a stream of argon gas, and residual chloroform was then removed after storage for 1 h under vacuum. Lipid films were then dissolved in 500 μL of potassium buffer (10 mM K_2HPO_4, 50 mM K_2SO_4, 5 mM MOPS, pH 7.4), as previously used for M2 structure and function studies,[17,18] and hydrated for 30 min at 5 °C above the phase transition temperature of the lipid mix, with vortex mixing every 5 min. Lipid solutions were then freeze-thawed 15 times, transferring between a dry ice ethanol bath and a water bath at hydration temperatures before extrusion using an Avanti Mini-Extruder, 26 times with membranes with a pore size of 100 nm (Whatman Nuclepore Track-Etched Membranes, GE Healthcare Bio-Sciences, Pittsburgh, PA, USA) at hydration temperatures. LUVs were stored at 4 °C and used within 1 week.

Fluorescence Polarization Anisotropy. 100 nM of M2AH FITC labeled peptide was mixed increasing concentrations of POPC:POPG LUVs (0−50 μM) containing either 0.5, 15, or 30 mol % cholesterol in Greiner Bio-One 96-well, black flat-bottomed plates. Fluorescence polarization anisotropy was determined on the FLUOstart Omega fluorescent plate reader (BMG Labtech, Bucks, U.K.), using a 482−16 nm excitation filter and a 530−40 nm band-pass emission filter. All data were blank-corrected before processing, and all experiments were performed with six repeats. Data was analyzed with GraphPad Prism 6 with K_d values determined by the least-squares regression model and significant differences determined by Welch's *t*-test of K_d.

Peptide Binding Assay. 100 μM of M2AH FITC labeled peptide was mixed with 2.5 mM of the indicated lipid vesicles and diluted with water to a final volume of 50 μL, as previously described.[18] Controls were made with 100 μM of M2AH FITC-labeled peptide and water. Samples were incubated for 1 h at room temperature in darkness to allow for peptide-membrane binding. After incubation, unbound peptide was removed by washing twice through 100 kDa Amicon Ultra centrifugal filters (Merck Millipore, Watford, U.K.). Retained fluorescence was determined on the FLUOstart Omega fluorescent plate reader, using a 492-nm excitation filter and a 520-nm band-pass emission filter. All data were blank-corrected before processing, and all experiments were performed in triplicate.

Tryptophan−Bromine Quenching Assay. 50 μM of F47W, Y52W, and F54W tryptophan-substituted M2AH peptides were incubated for 1 h with 2.5 mM of LUVs containing 0.5, 15, and 30 mol % cholesterol or with 2.5 mM of LUVs containing bromine-labeled POPC at either the 6,7 or 11,12 positions and containing either 0.5, 15, and 30 mol % cholesterol. The fluorescence emission spectra of the LUV solutions were collected between 300 and 400 at 1 nm intervals (λ excitation = 296 nm) in the presence and absence of M2AH-W peptide and the background LUV-only fluorescence was subtracted from the Typ fluorescence in the presence of peptide. The depth of insertion of the Typ reside
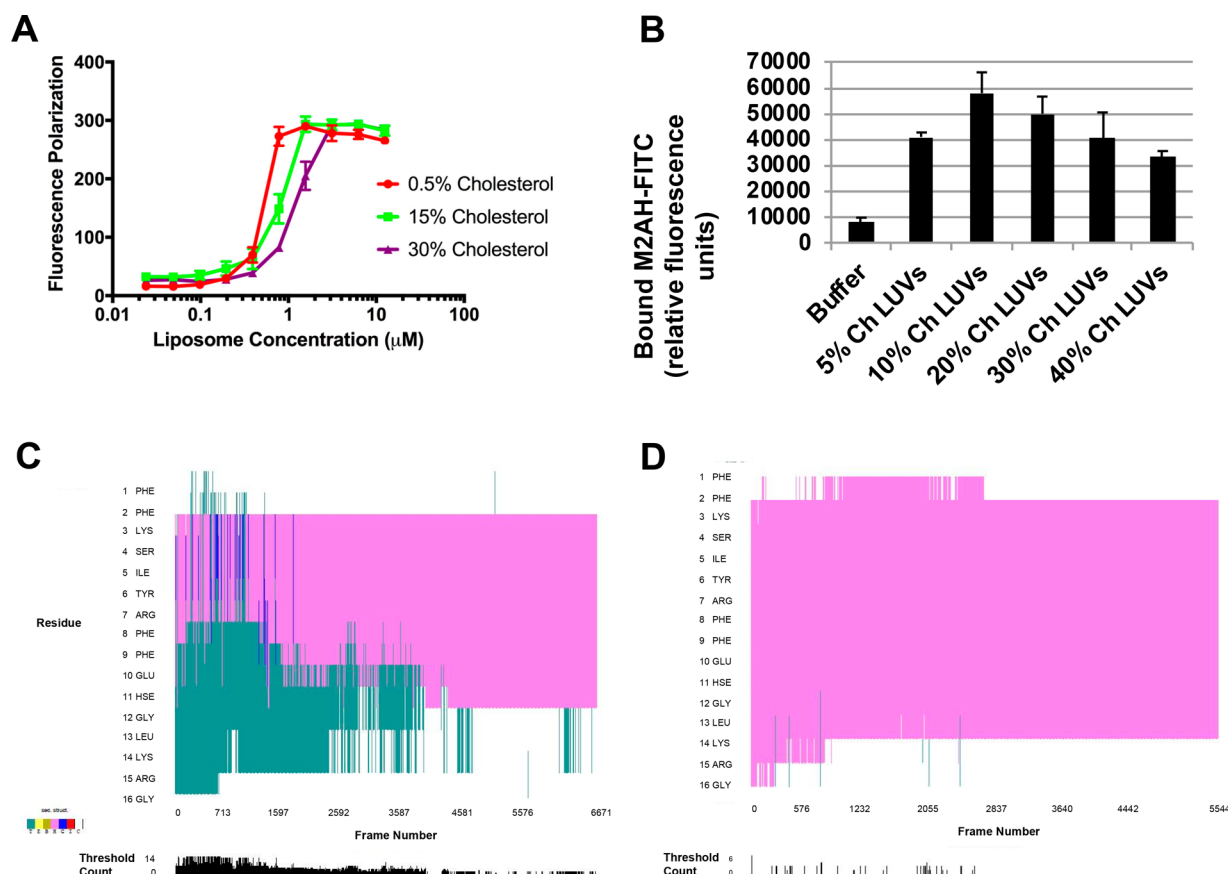
Figure 1. Minimal effect of membrane cholesterol on M2AH binding and secondary structure. (A) FITC-labeled M2AH peptide was incubated with increasing concentrations of LUVs containing 0.5, 15, or 30 mol % cholesterol and binding affinity was assessed by fluorescence polarization anisotropy. K_d values were determined by the least-squares regression model (0.67 μM at 0.5% cholesterol, 1.51 μM at 15% cholesterol, and 3.87 μM at 30% cholesterol) and the significant difference in K_d between 0.5% and 30% LUVs was determined by Welch's t-test of K_d ($p = 0.0128$). (B) FITC-M2AH was incubated with LUVs for 1 h before fluorescence was determined. Values represent the vesicle-bound fluorescence/background fluorescence and are means $\pm$ the standard deviation of three independent repeats. (C) MD simulation timeline of the helical secondary structure for the POPC/POPG simulation M2AH_3. The color-coded letters have the following meanings: T, Turn; E, Extended (β sheet); B, Bridge; H, α helix; G, 310-helix; I, PI-helix; and C, coil (none of the above). (D) Timeline of the helical secondary structure for the POPC/POPG/CHLsimulation M2AH_CHL_3.

in the membrane was calculated using the modified parallax method:[31]

$$Z_{CF} = L_{C1} + \frac{\left(-\frac{1}{\pi C}\right) \ln \frac{F_1}{F_2} - L_{21}^2}{2L_{21}}$$

where Z_{CF} is the distance of Typ residue from the center of the bilayer, L_{C1} the distance between the 6,7 Br atom and the bilayer center, and L_{21} the distance between the 6,7 Br atom and the 11,12 Br atom. F_1 is the Typ fluorescence intensity in the presence of the 6,7 Br atom (λ emission = 338 nm), and F_2 is the Typ fluorescence intensity in the presence of the 11,12 Br atom (λ emission = 338 nm). C is the two-dimension (2D) concentration of Br atoms in the membrane plane (mole fraction per unit area of Br-lipid/total lipid). Values for L_{C1} (10.8 Å), L_{21} (4.5 Å), and C (0.3/70 Å²) have been previously determined from X-ray diffraction (XRD) experiments.[32,33]

Laurdan Assay. 2.5 mM of LUVs were mixed with 25 μM Laurdan dye (Life Technologies, Paisley, U.K.) and 200 μM of peptide, where indicated, in a total volume of 50 μL, as previously described.[17] Fluorescence was measured on a Cary Eclipse fluorescence spectrophotometer (Agilent Technologies, CA, USA) using a 355 nm excitation filter recording

fluorescence emissions at 440 and 490 nm. All experiments were performed in triplicate. The Laurdan General Polarization (GP) value was calculated using the equation[34]

$$GP = \frac{I_{440} - I_{490}}{I_{440} + I_{490}}$$

Molecular Dynamics Simulations. *Peptide Model.* The three-dimensional (3D) structure of the α-helical Udorn M2 amphipathic helix (M2AH) peptide is taken from the NMR ensemble and converted to CHARMM residue types. This involves reassigning atom labels and making protonation states consistent with predictions (ProPKA is used[35]); in particular, lysines (residues 3 and 14) and arginines (residues 7 and 15) have positively charged side chains (standard LYS and ARG types), the glutamic acid (residue 10) has a negatively charged side chain (GLU type), histidine (residue 11) has a neutral side chain (HSE type). Standard N-terminal (NTERM, $-NH_3^+$) and C-terminal (CTERM, $-COO-$) patches are used. No further post-translational or chemical modifications are applied.

System Setup. A single peptide per simulation box was positioned by placing it parallel to the membrane plane and translating it by 10, 15, 20, 25, or 30 Å, relative to the
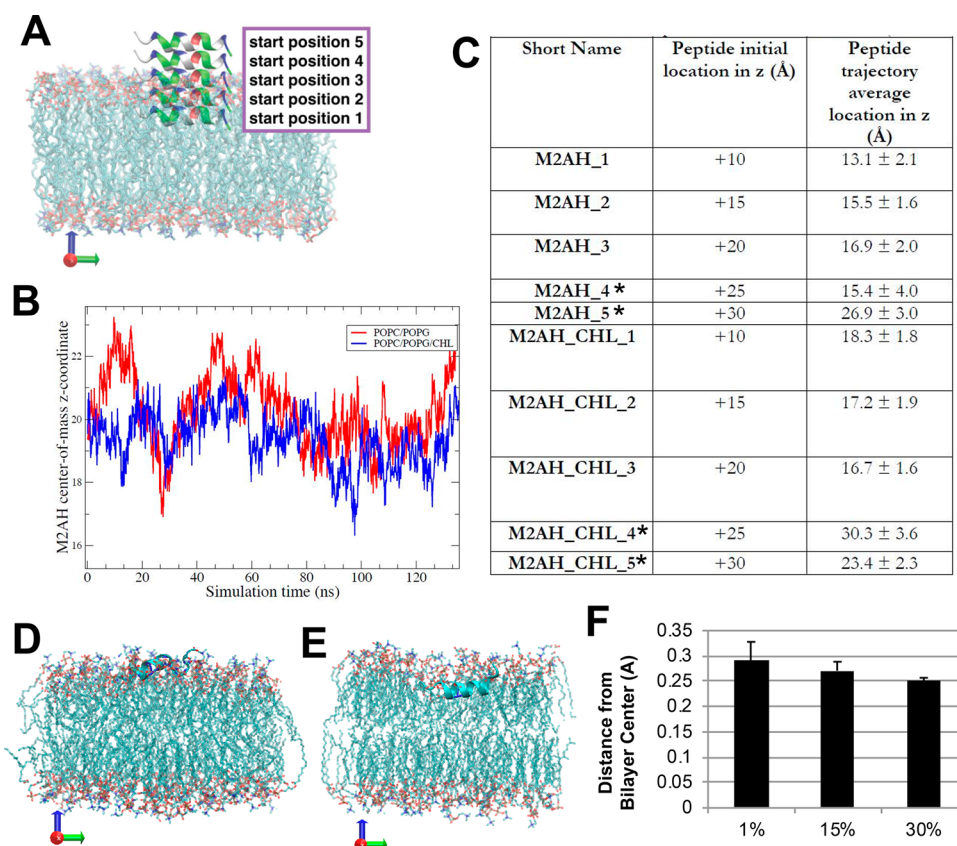
Figure 2. Cholesterol modulates the M2AH depth of insertion. Molecular dynamics (MD) simulations of the M2AH peptide and different lipid bilayers. (A) Side view of initial configurations chosen for the M2AH/bilayer simulations. Each starting position corresponds to a translation along the z-axis, according to the values specified in panel (C). The M2AH peptides are otherwise positioned in the same orientation, with respect to the bilayer membrane. (B) Representative penetration depth during simulation extracted from the peptide center of mass, relative to the membrane center of mass. Trajectories M2AH_3 and M2AH_CHL_3 are shown, which are started at a z-axis offset of +2 nm. (C) Average peptide Z-location from different starting configurations. Note that trajectories 4 and 5 did not bind consistently and are not used for analyses (indicated by an asterisk (*)). (D) Representative snapshots of M2AH peptide in POPC:POPC bilayer simulations (from M2AH_3) and (E) POPC:POPG:cholesterol bilayers (from M2AH_CHL_3). (F) 50 μM Y25W tryptophan-substituted M2AH peptide was incubated for 1 h with 2.5 mM LUVs containing 1, 15, and 30 mol % cholesterol and with cholesterol-varied LUVs containing bromine-labeled POPC at either the 6,7 or 11,12 positions. The tryptophan fluorescence spectra were collected (Figure S2) and used to calculate the distance from the center of the membrane bilayer. Values are shown as means ± standard deviation. No significant differences were observed between peptide insertion depth in 1 mol % cholesterol membranes and 30 mol % membranes, with a Student's t-test value of $p = 0.69$.

membrane center ($z = 0$) in an orientation consistent with the estimated (using HELIQUEST[36]) helical hydrophobic momentum vector, μ, which dictates the amphipathicity of the helix.[37] Physiological salt (150 mM KCl) is added to all simulations by replacing randomly chosen water molecules with K^+ or Cl^- ions. Two types of model lipid membranes are investigated. The first is a POPC/POPG (80/20 component ratio in both leaflets), and the second has cholesterol (CHL) added, POPC/POPG/CHL (50/20/30 component ratio in both leaflets). For more details, see the Supporting Information.

Simulation Protocol. We use a standard simulation protocol dictated by best practices: NPT ensemble (Nosé–Hoover thermostat set to 300 K,[38,39] semiisotropic Parrinello–Rahman barostat set to 1 atm),[40] LINCS constraints in H atoms,[41,42] 2 fs integration time steps, particle-mesh Ewald summation for electrostatic interactions,[43] Force-switch starting at 1.0 nm to a cutoff at 1.2 nm. The simulation time is ~300–600 ns per trajectory. We use the CHARMM-GUI[44] membrane builder[45,46] to initialize the geometries. GROMACS (version 5.0)[47] is used to perform the MD simulations, CHARMM36 force field is used for the proteins[48] and lipids[49]

with the TIP3P water model.[50] VMD[51] is used for analysis and visualization. The recommended stepwise relaxation scheme, which consists of minimization (step 6.0), equilibration (steps 6.1 through 6.6) before the production run, is started. Note that the simulation temperature was chosen to match previous biological experiments and, therefore, is not performed at physiological temperature. However, the properties of our model membranes are only weakly dependent on temperature within this range.[52]

Analysis Details. The helix angle is calculated by projecting the directional vector from the α-C atom of Lys3 to His11 (exactly two helix turns away) onto the simulation box z-axis vector. The penetration depth is monitored by following the z-coordinate of residue Phe8. The secondary structure in the peptide is monitored using the STRIDE algorithm.[53] Salt bridges are determined based on an O–N geometric bond distance cutoff criterion of 3.2 Å. Hydrogen bonds are determined based on a geometric bond distance cutoff of 3.0 Å and a bond angle cutoff of 20°. The packing analysis was performed as previously described.[54,55] In short, the area of the lipid head groups was projected down to the gridded x/y plane, and the points corresponding to hydrophobic defects were
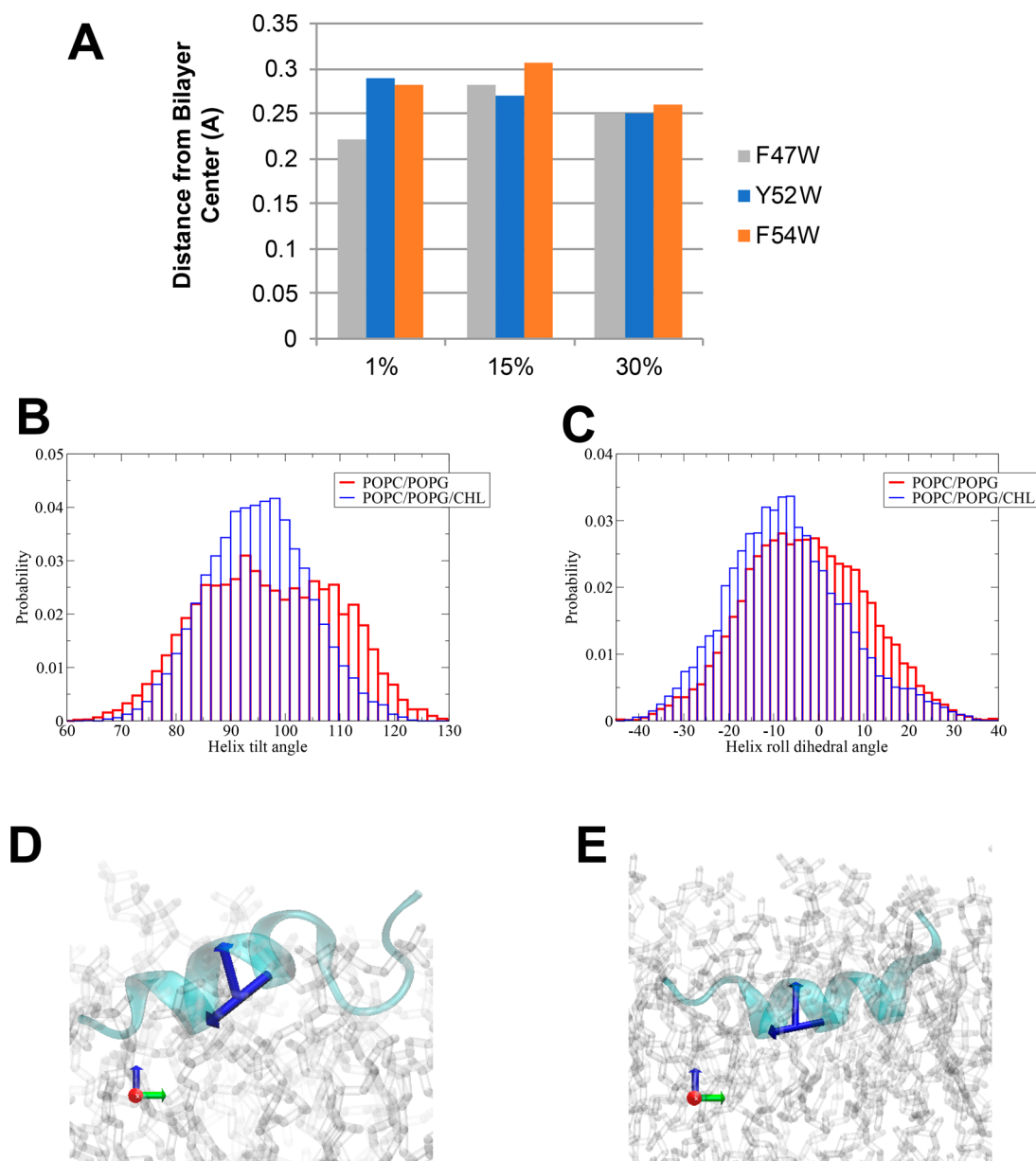
Figure 3. Cholesterol-dependent orientation of membrane-bound M2AH. (A) 50 μM F47W, Y52W, and F54W tryptophan-substituted M2AH peptides were incubated for 1 h with 2.5 mM LUVs containing 0.5, 15, and 30 mol % cholesterol and with cholesterol-varied LUVs containing bromine-labeled POPC at either the 6,7 or 11,12 positions. The tryptophan fluorescence spectra were collected and used to calculate the distance from the center of the membrane bilayer. (B) MD simulation showing binned angles during the simulated trajectories (for trajectories 1−3). 90° corresponds to the horizontal starting positions. (C) Binned roll angles during the simulated trajectories (for trajectories 1−3). (D) Peptide orientations are shown in representative snapshots of the M2AH peptide in POPC:POPC bilayer simulations (M2AH_3) and (E) POPC:POPG:cholesterol bilayers (M2AH_CHL_3).

clustered and measured to determine the size of the individual clusters.

RESULTS

Minimal Effect of Membrane Cholesterol on M2AH Binding and Secondary Structure. Previous results have shown that the M2AH forms an helical structure upon membrane binding.[17] If cholesterol concentrations modulate M2AH binding, this could directly impact domain formation and the ability to alter membrane curvature. Thus, we first determined the association of a FITC-tagged M2AH peptide with POPC:POPG LUVs with a range of membrane cholesterol concentrations, using fluorescence polarization

anisotropy. Liquid-disordered POPC:POPG membranes and a nonpalmitoylated C50S M2AH peptide were specifically chosen, because they represent a widely used model system for evaluating the impact of cholesterol on M2AH structure and function.[2,17,18,26,27,30] We see that the affinity of M2AH peptide binding to LUVs is slightly, but significantly, inversely correlated with increasing cholesterol concentrations (Figure 1a), with calculated K_d values of 0.67 μM at 0.5% cholesterol, 1.51 μM at 15% cholesterol, and 3.87 μM at 30% cholesterol (p-value, 0.5% vs 30%, is 0.0128). This is comparable to previous work with other amphipathic peptides, where cholesterol caused an overall increase in peptide binding but a decrease in overall binding affinity.[56] We also assessed

M2AH membrane binding by incubating FITC-M2AH peptide with LUVs, removing unbound peptide by spin filtration and quantifying the bound fluorescent signal. We see comparable peptide binding to LUVs containing 5% and 30% cholesterol, although binding is slightly increased at 10% (see Figure 1b).

To determine if cholesterol affects M2AH α-helix secondary structure formation, we attempted to determine the NMR structure of the M2AH bound to high- and low-cholesterol LUV membranes. Our previous results have determined the low-cholesterol NMR structure of the M2AH;[17] however, when bound to 30% cholesterol LUVs, the peptide-transferred NOE NMR signal is lost, suggesting possible changes in M2AH K_{off} rates, although these were not assessed in this study. Instead, we have used all-atom molecular dynamics (MD) simulations to investigate modeled M2AH secondary structure changes over time on POPC:POPG bilayers, compared to POPC:POPG bilayers containing 30% cholesterol (see Figure S1 in the Supporting Information). Our results show that M2AH forms a stable α-helix secondary structure under both membrane conditions, in a manner similar to that observed in previously reported results with other amphipathic peptides,[56] although there seems to be more structural fluctuations and flexibility of the M2 α-helix in the absence of cholesterol (Figure 1c and 1d). Together, these results suggest that the ability of cholesterol to modulate M2AH activity is not strongly affected by differential membrane binding or the induction of a secondary structure.

Membrane Cholesterol Alters the Depth and Angle of M2AH-Membrane Insertion. While cholesterol may not strongly impact M2AH-membrane binding, cholesterol may modulate the orientation of the peptide within the membrane, with subsequent effects on activity. In order to estimate the depth of M2AH membrane insertion and the effect of membrane cholesterol, we first performed MD simulations, examining the behavior of the modeled peptide on POPC:POPG bilayers, compared to POPC:POPG bilayers containing 30% cholesterol. Analysis of multiple repeated simulations showed that the M2AH peptide was more frequently found slightly deeper within the membrane (toward the bilayer midplane) when 30% cholesterol was present (see Figures 2a–e). These results were further examined by using tryptophan (Typ) fluorescence quenching by bromine-labeled lipids to determine the depth of peptide insertion in the membrane. The M2AH peptide was substituted with Y52W to enable Typ fluorescence measurements. Typ fluorescence is sensitive to the presence of bromine, thus lipids with Br conjugated to the 6–7 lipid tail position, the 9–10 position, or the 11–12 position were used to estimate the depth of M2AH insertion. For reference, Br-6,7 conjugated lipids will quench Typ fluorescence when it is below the level of the lipid headgroups but not when it is at the level of the headgroups or on the surface of the membrane. The M2AH-Y52W peptide was added to LUVs containing Br-6,7-PC or Br-11,12-PC with 1%, 15%, or 30% cholesterol, the Typ fluorescence spectra were collected (see Figure S2 in the Supporting Information) and used to calculate the distance of the Typ residue from the bilayer center, using the modified parallax equation.[57] These results also showed a slight, but nonstatistically significant, difference in membrane penetration depth, suggesting that membrane cholesterol levels do not significantly alter M2AH Z positioning in the membrane (see Figure 2f).

To examine if cholesterol affects the angle of the peptide within the membrane, we expanded our Typ quenching experiments by using M2AH peptides with Typ substitutions at different points along the length of the helix. Using our previous saturation transfer difference NMR experiments as a guide for peptide–membrane interactions, we selected three bulky hydrophobic residues that would likely be compatible with Typ substitutions without affecting membrane binding or secondary structure.[17] The M2AH peptide was substituted with either F47W, Y52W, or F54W, and each different M2AH-W peptide was added to LUVs containing Br-6,7-PC or Br-11,12-PC with 1%, 15%, or 30% cholesterol; the Typ fluorescence spectra were collected (Figure S2) and used to calculate the distance of the Typ residue from the bilayer center. As with the Y52W substitution, we did not detect a difference between the average depth of the W47 or W54 residues (see Figure 3a). However, N-terminal residues (e.g., W47) of the peptide showed increased depth in the membrane at low-cholesterol concentrations, compared to C-terminal residues, whereas at high cholesterol concentrations, all residues showed comparable depths (Figure 3a). This suggests that cholesterol may affect the orientation of M2AH in the membrane. These results are supported by the MD simulations, which showed that M2AH was most frequently found oriented at ~92° from the bilayer normal (inclination in the Z-axis) in the absence of cholesterol, but at ~98°, in the presence of cholesterol (see Figures 3b, 3d, and 3e). In addition, the presence of cholesterol causes a ~10° counterclockwise rotation of the helix within the membrane (Figure 3c). Together, these results show that cholesterol affects the positioning of the M2AH within the membrane. The key amino acid residue of M2AH in most-frequent direct contact with cholesterol was identified in the MD simulations as F54, which inserts deeply into the membrane (see Figure S3a in the Supporting Information). Because of the secondary helical structure of the peptide, residues that are four positions upstream and downstream (C50 and G58/L59, respectively) also showed increased contact with cholesterol (see Figure S3a). No stereospecific interactions between M2AH and cholesterol were observed. Furthermore, the cholesterol hydroxyl group does not appear to form a stable hydrogen bond to the peptide (including its backbone) and, as such, likely has little influence on the peptide structure. Instead, the dominant interaction between M2AH and cholesterol is found to be a hydrophobic stacking interaction between F54 and the hydrocarbon rings of cholesterol (see Figure S3b in the Supporting Information). Per-residue contacts between M2AH and POPC/POPG lipids were quantified in the presence and absence of cholesterol, with only minor differences being observed (see Figures S3c and S3d in te Supporting Information). Interactions between counterions and the phospholipids were also examined, with counterions coordinating closer around the phospholipids in the presence of cholesterol, especially with POPG (Figures S3e and S3f in the Supporting Information). This suggests that cholesterol affects the positioning of M2AH, which may then affect the positioning of the lipid headgroups.

Cholesterol Limits M2AH-Induced Lipid Headgroup Separation Required for Curvature and Membrane Scission. Changes in AH domain membrane insertion can have significant impacts on lipid headgroup separation and affect the ability to alter membrane curvature and cause scission. To assess the effects of cholesterol on M2AH's ability to alter lipid headgroup separation, we used MD simulation to assess the likelihood of given distances of separation between

lipid headgroup P atoms (PC—PC, PC—PG, or PG—PG) in the presence and absence of cholesterol. The results show that, while M2AH induces minimal changes in the separation between PC—PC and PC—PG headgroups, M2AH causes a decrease in PG—PG P atom distances in the presence of 30% cholesterol, but no change in distances in the absence of cholesterol (Figure 4a). The differential effect on PG instead of
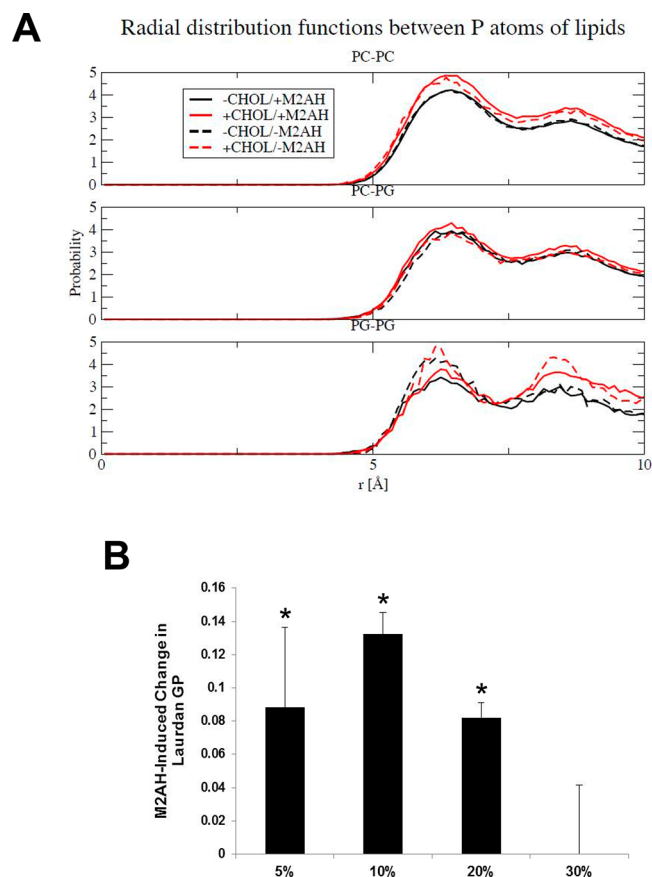

Figure 4. Cholesterol modulates the ability of M2AH to induce lipid order. (A) MD simulation RDFs of P atom pair distributions between POPC—POPC (top), POPC—POPG (middle), and POPG—POPG (bottom). Results are averaged over trajectories 1−3. (B) 2.5 mM LUVs containing 5, 10, 20, or 30 mol % cholesterol were incubated for 1 h with 25 μM Laurdan dye in the presence or absence of increasing amounts of M2AH peptide. Laurdan fluorescence was then measured at 440 and 490 nm, and the ratio was used to calculate the Laurdan GP. Values are shown as GP(M2AH-LUVs) − GP(LUVs) and are the mean ± standard deviation of three independent repeats. Asterisk symbol (*) indicates a statistically significant change in GP upon peptide insertion, with a Student's t test value of $p < 0.05$. No significant change in GP was seen with 30% cholesterol LUVs, $p = 0.996$.

PC may be attributed to the strong interaction of the cationic surface of the M2AH with charged anionic lipids such as PG.[17] Interestingly, the presence of cholesterol itself caused a separation of PG headgroups (Figure 4a), and it is possible that this separation increases lipid phase separation while the ability of M2AH to cluster PG headgroups mitigates this effect, slightly reducing the strain on the membrane in the presence of 30% cholesterol and reducing M2AH scission activity.

M2AH-induced changes in lipid packing may further affect the ability of the domain to induce lipid ordering. As lipid ordering has been shown to affect line tension and membrane

scission, alterations of M2AH-induced lipid ordering could have significant impacts on virus budding.[17] To investigate if cholesterol alters M2AH induction of lipid ordering, we added M2AH peptide to Laurdan-labeled LUVs and assessed changes in the GP function of the dye. Laurdan is a hydrophobic dye that incorporates into the lipid bilayer at the lipid tails and undergoes emission spectrum shifts based on the exposure of the dye to polar media; therefore increases in Laurdan GP indicate a decrease in exposure of the dye to the aqueous environment caused by an increase in lipid order and lipid packing. We see that the addition of the M2AH peptide to Laurdan-containing LUVs causes a statistically significant increase in lipid order in low-cholesterol LUV (Figure 4b). However, in the presence of 30% cholesterol, the M2AH peptide is no longer able to alter lipid order, suggesting that orientation of the peptide in the membrane may affect lipid packing and, thus, modulate M2AH activity.

■ DISCUSSION AND CONCLUSIONS

The M2AH is a membrane-active domain that has been shown to bind membranes and alter curvature in a cholesterol-dependent process that is essential for membrane scission and the release of budding influenza virions.[2,12,13] Cholesterol has been previously shown to bind to the M2 protein at multiple sites,[26] including residues F47, F54, and R61 of the AH domain.[27] In high levels of membrane cholesterol (>20%), M2AH loses its ability to alter membrane curvature and cause scission in vesicle models,[2] although the specific biological effect of cholesterol on M2AH activity remains unclear. In this study, we have investigated the effect of cholesterol on the ability of the M2AH to associate with and modify model membranes.

The M2AH binds to a variety of biological membranes and is structured into an α-helix only upon membrane binding.[17] Here we show that the presence of 30% cholesterol, in LUV membranes, has minimal impact on M2AH membrane binding (Figures 1a and 1b) and slightly increases the speed of α-helix formation upon membrane contact (Figures 1c and 1d). These results agree with previous ssNMR experiments that showed comparable α-helix formation and association of the AH domain with membranes of increasing cholesterol concentration.[28,29] This suggests that cholesterol does not strongly affect M2AH binding or secondary structure formation, though the helix was found to be more stable[28] and more tightly packed in the presence of cholesterol.[29] It is possible this change in M2AH packing density would affect protein clustering, increasing the "effective" local concentration in the membrane and inducing membrane curvature, as has been previously shown through ssNMR and MD simulations with the full-length M2 protein,[11,58] although the direct effects of cholesterol on M2 clustering have yet to be proven.

While cholesterol does not affect membrane binding by M2AH, it may slightly affect the depth of membrane insertion of the domain and significantly alter its orientation within the membrane. MD modeling and Typ bromine quenching experiments show that the M2AH is inserted at a comparable or slightly deeper depth in the membrane in the presence of cholesterol (see Figure 2), this contrasts with previous ssNMR studies that showed the AH domain is somewhat less buried in the membrane in the presence of cholesterol.[29] However, the ssNMR experiments were performed with a M2 TMD-AH construct and it is likely that the presence of the TMD affects the depth of AH membrane insertion. The study also found

that cholesterol changed the angle and rotation of the helix within the membrane.[29] Our results confirm and expand these observations by demonstrating cholesterol-induced changes in the angle and rotation of the helix, relative to the bilayer normal. At high levels of membrane cholesterol, the AH is oriented parallel to the membrane, whereas in low levels of cholesterol, the M2AH undergoes a ∼6° tilt and is now angled in the membrane, along with a ∼10° rotation of the helix that may change the ability of the M2AH to modify membrane properties (Figure 3). AH domains inserted in the membrane are known to have different biological effects that are dependent on the helix orientation in the membrane. Many cell-penetrating antimicrobial peptides alter membrane curvature: at low concentrations, they bind parallel to the membrane, and at high concentrations, these peptides often change their orientation in the membrane, so that the helix is now perpendicular to the membrane and can form pores.[59] While the effect of concentration on the M2AH membrane orientation has never been assessed, the ∼6° change in angle of the M2AH (Figure 3) does not appear to be sufficient to form pores in the membrane. However, the M2AH can cause membrane leakage in vesicles and the range of biological activity of the M2AH, from leakage to curvature and scission, may be dependent on peptide orientation in the membrane.[2,29,58]

Here, our results show that cholesterol alters the orientation of the M2AH peptide, which then mediates different biophysical effects on the membrane. In low-cholesterol membranes, insertion of the angled M2AH peptide causes changes in lipid tail packing that result in increased lipid order,[17] and likely increase membrane line tension[11] (Figure 4b). In contrast, in high levels of cholesterol, modeling suggests that there is increased separation of anionic lipid headgroups. In this environment, the membrane-parallel insertion of the M2AH peptide reduces headgroup separation and does not affect lipid order (Figures 4a and 4b). It is possible that M2AH cannot further increase lipid order beyond the contribution of 30% cholesterol, which is known to increase lipid order.[60] High membrane cholesterol levels, and the associated lipid headgroup separation,[60] may also enable peptide binding without disruption of membrane structure, as has been shown for other AH-containing antimicrobial peptides.[56]

M2 has been shown to cluster and mediate membrane scission at lipid phase boundaries, acting as a linactant and likely using the line tension energy between the lipid phases to drive membrane scission.[2,11,58,61] Recent results have validated these predictions by showing that increasing membrane stress facilitates M2 induction of membrane curvature.[11] Thus, alteration of either lipid headgroup separation or lipid order and membrane tension can be sufficient to alter membrane curvature and cause scission, thus suggesting a mechanism action for the M2AH.[62−64] However, given that cholesterol can be an organizing factor in lipid raft formation, which would increase local membrane tension, it is rather surprising that, in lipid vesicle systems, high levels of membrane cholesterol inhibit scission activity, instead of promoting activity.[2] It is possible that this discrepancy is dependent on the activity of cholesterol in different membrane model systems. In single lipid phases, cholesterol increases lipid mixing and decreases the size of lipid nanodomains, effectively reducing nanodomain line tension, whereas with lipid mixtures that can phase separate, increasing cholesterol in the gel phase beyond 16%

causes the formation of Lo phases.[65] Thus, cholesterol may both affect the orientation of the M2AH domain in the membrane and affect membrane tension levels (which M2AH uses to drive membrane scission), with differential effects of cholesterol in single lipid phases, phase-separated lipids, and in biological membranes with structured lipid domains. Further research is necessary to determine the specific impact of cholesterol on M2AH orientation and function in these different biological membranes.

In the context of the full-length M2 protein, the AH domain is but one membrane-active region. It has been shown that the TMD also possesses curvature-altering abilities and the AH domain is more effective in the full-length protein,[12] possibly because the native tetramer form of the protein enhances the effective concentration of the AH domain, or because the anchoring of one end of the AH affects the subsequent angle of membrane insertion and, thus, biological activity. Further work is needed in order to determine how the structure of the AH domain is affected by its N-terminal anchoring to the TMD and how cholesterol modifies domain orientation and function in the context of the full-length protein. All of these components are inter-related, and a full understanding of M2-mediated scission will be required to understand the sum of the parts. Here, our data suggest that cholesterol modifies M2-mediated membrane scission by altering the angle and depth of helix membrane insertion, affecting the formation of lipid packing defects and the induction of line tension between lipid phases. This may allow for spatial-temporal control over the budding process, balancing M1 interactions during assembly with the mediation of scission during virus release.[28]

■ ASSOCIATED CONTENT

ⓈI Supporting Information

The Supporting Information is available free of charge at https://pubs.acs.org/doi/10.1021/acs.jpcb.0c03331.

Overview of the MD simulation used in Figures 1c, 1d, 2a−e, 3b−e, and 4a (Figure S1); tryptophan fluorescence spectra used in Figures 2f and 3a (Figure S2); per-residue contacts between M2AH and lipids, as well as lipid−counterion contacts and radial distribution functions (Figure S3) (PDF)

■ AUTHOR INFORMATION

Corresponding Authors

Jeremy S. Rossman − School of Biosciences, University of Kent, Canterbury, Kent CT2 7NJ, United Kingdom; ⓘ orcid.org/0000-0001-6124-4103; Phone: +44 (0)1227 823206; Email: j.s.rossman@kent.ac.uk

Gregory A. Voth − Department of Chemistry and Chicago Center for Theoretical Chemistry, James Franck Institute, and Institute for Biophysical Dynamics, The University of Chicago, Chicago, Illinois 60637, United States; ⓘ orcid.org/0000-0002-3267-6748; Phone: +1 773-702-9092; Email: gavoth@uchicago.edu

Authors

Agnieszka Martyna − School of Biosciences, University of Kent, Canterbury, Kent CT2 7NJ, United Kingdom

Basma Bahsoun − School of Biosciences, University of Kent, Canterbury, Kent CT2 7NJ, United Kingdom

Jesper J. Madsen − Department of Chemistry and Chicago Center for Theoretical Chemistry, James Franck Institute, and

Institute for Biophysical Dynamics, The University of Chicago, Chicago, Illinois 60637, United States; Department of Global Health, College of Public Health, University of South Florida, Tampa, Florida 33612, United States; ● orcid.org/0000-0003-1411-9080

Frederic St. J. S. Jackson − School of Biosciences, University of Kent, Canterbury, Kent CT2 7NJ, United Kingdom

Matthew D. Badham − School of Biosciences, University of Kent, Canterbury, Kent CT2 7NJ, United Kingdom

Complete contact information is available at:
https://pubs.acs.org/10.1021/acs.jpcb.0c03331

Author Contributions

∇These authors contributed equally to this work.

Notes

The authors declare no competing financial interest.

■ REFERENCES

(1) Rossman, J. S.; Lamb, R. A. Influenza virus assembly and budding. *Virology* **2011**, *411* (2), 229−236.

(2) Rossman, J. S.; Jing, X.; Leser, G. P.; Lamb, R. A. The influenza virus M2 protein mediates ESCRT-independent membrane scission. *Cell* **2010**, *142* (6), 902−913.

(3) Lamb, R. A.; Pinto, L. H. The proton selective ion channels of influenza A and B viruses. In *Contemporary Topics in Influenza Virology*; Kawaoka, Y., Ed.; Horizon Scientific Press: Wymondham, Norfolk, U.K., 2005; pp 65−93.

(4) Pinto, L. H.; Lamb, R. A. The M2 proton channels of influenza A and B viruses. *J. Biol. Chem.* **2006**, *281*, 8997−9000.

(5) Liang, R.; Swanson, J. M. J.; Madsen, J. J.; Hong, M.; DeGrado, W. F.; Voth, G. A. Acid activation mechanism of the influenza A M2 proton channel. *Proc. Natl. Acad. Sci. U. S. A.* **2016**, *113* (45), E6955−E6964.

(6) Watkins, L. C.; Liang, R.; Swanson, J. M. J.; DeGrado, W. F.; Voth, G. A. Proton-Induced conformational and hydration dynamics in the influenza A M2 channel. *J. Am. Chem. Soc.* **2019**, *141* (29), 11667−11676.

(7) Torabifard, H.; Panahi, A.; Brooks, C. L. M2 amphipathic helices facilitate pH-dependent conformational transition in influenza A virus. *Proc. Natl. Acad. Sci. U. S. A.* **2020**, *117* (7), 3583−3591.

(8) Chen, B. J.; Leser, G. P.; Jackson, D.; Lamb, R. A. The influenza virus M2 protein cytoplasmic tail interacts with the M1 protein and influences virus assembly at the site of virus budding. *J. Virol.* **2008**, *82*, 10059−10070.

(9) Rossman, J. S.; Jing, X.; Leser, G. P.; Balannik, V.; Pinto, L. H.; Lamb, R. A. Influenza virus M2 ion channel protein is ncecessary for filamentous virion formation. *J. Virol.* **2010**, *84* (10), 5078−5088.

(10) Schroeder, C. Cholesterol-binding viral proteins in virus entry and morphogenesis. *Subcell. Biochem.* **2010**, *51*, 77−108.

(11) Madsen, J. J.; Grime, J. M. A.; Rossman, J. S.; Voth, G. A. Entropic forces drive clustering and spatial localization of influenza A M2 during viral budding. *Proc. Natl. Acad. Sci. U. S. A.* **2018**, *115* (37), E8595−E8603.

(12) Schmidt, N. W.; Mishra, A.; Wang, J.; DeGrado, W. F.; Wong, G. C. Influenza virus A M2 protein generates negative Gaussian membrane curvature necessary for budding and scission. *J. Am. Chem. Soc.* **2013**, *135* (37), 13710−9.

(13) Roberts, K. L.; Leser, G. P.; Ma, C.; Lamb, R. A. The amphipathic helix of influenza A virus M2 protein is required for filamentous bud formation and scission of filamentous and spherical particles. *J. Virol.* **2013**, *87* (18), 9973−82.

(14) Nguyen, P. A.; Soto, C. S.; Polishchuk, A.; Caputo, G. A.; Tatko, C. D.; Ma, C.; Ohigashi, Y.; Pinto, L. H.; DeGrado, W. F.; Howard, K. P. pH-induced conformational change of the influenza M2 protein C-terminal domain. *Biochemistry* **2008**, *47*, 9934−9936.

(15) Schnell, J. R.; Chou, J. J. Structure and mechanism of the M2 proton channel of influenza A virus. *Nature* **2008**, *451*, 591−595.

(16) Tian, C.; Gao, P. F.; Pinto, L. H.; Lamb, R. A.; Cross, T. A. Initial structural and dynamic characterization of the M2 protein transmembrane and amphipathic helices in lipid bilayers. *Protein Sci.* **2003**, *12*, 2597−2605.

(17) Martyna, A.; Bahsoun, B.; Badham, M. D.; Srinivasan, S.; Howard, M. J.; Rossman, J. S. Membrane remodeling by the M2 amphipathic helix drives influenza virus membrane scission. *Sci. Rep.* **2017**, *7*, 44695.

(18) Martyna, A.; Gomez-Llobregat, J.; Linden, M.; Rossman, J. S. Curvature sensing by a viral scission protein. *Biochemistry* **2016**, *55* (25), 3493−6.

(19) Wang, T.; Hong, M. Investigation of the curvature induction and membrane localization of the influenza virus m2 protein using static and off-magic-angle spinning solid-state nuclear magnetic resonance of oriented bicelles. *Biochemistry* **2015**, *54* (13), 2214−26.

(20) Rossman, J. S.; Lamb, R. A. Viral membrane scission. *Annu. Rev. Cell Dev. Biol.* **2013**, *29*, 551−69.

(21) Schroeder, C.; Heider, H.; Moncke-Buchner, E.; Lin, T. I. The influenza virus ion channel and maturation cofactor M2 is a cholesterol-binding protein. *Eur. Biophys. J.* **2005**, *34*, 52−66.

(22) Thaa, B.; Levental, I.; Herrmann, A.; Veit, M. Intrinsic membrane association of the cytoplasmic tail of influenza virus M2 protein and lateral membrane sorting regulated by cholesterol binding and palmitoylation. *Biochem. J.* **2011**, *437* (3), 389−397.

(23) Stewart, S. M.; Wu, W. H.; Lalime, E. N.; Pekosz, A. The cholesterol recognition/interaction amino acid consensus motif of the influenza A virus M2 protein is not required for virus replication but contributes to virulence. *Virology* **2010**, *405* (2), 530−538.

(24) Oates, J.; Watts, A. Uncovering the intimate relationship between lipids, cholesterol and GPCR activation. *Curr. Opin. Struct. Biol.* **2011**, *21* (6), 802−7.

(25) Li, C.; Qin, H.; Gao, F. P.; Cross, T. A. Solid-state NMR characterization of conformational plasticity within the transmembrane domain of the influenza A M2 proton channel. *Biochim. Biophys. Acta, Biomembr.* **2007**, *1768* (12), 3162−70.

(26) Ekanayake, E. V.; Fu, R.; Cross, T. A. Structural influences: cholesterol, drug, and proton binding to full-length influenza A M2 protein. *Biophys. J.* **2016**, *110* (6), 1391−9.

(27) Elkins, M. R.; Williams, J. K.; Gelenter, M. D.; Dai, P.; Kwon, B.; Sergeyev, I. V.; Pentelute, B. L.; Hong, M. Cholesterol-binding site of the influenza M2 protein in lipid bilayers from solid-state NMR. *Proc. Natl. Acad. Sci. U. S. A.* **2017**, *114* (49), 12946−12951.

(28) Liao, S. Y.; Fritzsching, K. J.; Hong, M. Conformational analysis of the full-length M2 protein of the influenza A virus using solid-state NMR. *Protein Sci.* **2013**, *22* (11), 1623−38.

(29) Kim, S. S.; Upshur, M. A.; Saotome, K.; Sahu, I. D.; McCarrick, R. M.; Feix, J. B.; Lorigan, G. A.; Howard, K. P. Cholesterol-dependent conformational exchange of the C-terminal domain of the influenza A M2 protein. *Biochemistry* **2015**, *54* (49), 7157−67.

(30) Herneisen, A. L.; Sahu, I. D.; McCarrick, R. M.; Feix, J. B.; Lorigan, G. A.; Howard, K. P. A Budding-defective M2 mutant exhibits reduced membrane interaction, insensitivity to cholesterol, and perturbed interdomain coupling. *Biochemistry* **2017**, *56* (44), 5955−5963.

(31) Donate, F.; Yanez, A. J.; Iriarte, A.; Martinez-Carrion, M. Interaction of the precursor to mitochondrial aspartate aminotransferase and its presequence peptide with model membranes. *J. Biol. Chem.* **2000**, *275* (44), 34147−56.

(32) McIntosh, T. J.; Holloway, P. W. Determination of the depth of bromine atoms in bilayers formed from bromolipid probes. *Biochemistry* **1987**, *26* (6), 1783−8.

(33) Lewis, B. A.; Engelman, D. M. Lipid bilayer thickness varies linearly with acyl chain length in fluid phosphatidylcholine vesicles. *J. Mol. Biol.* **1983**, *166* (2), 211−7.

(34) Parasassi, T.; De Stasio, G.; d'Ubaldo, A.; Gratton, E. Phase fluctuation in phospholipid membranes revealed by Laurdan fluorescence. *Biophys. J.* **1990**, *57* (6), 1179−86.

(35) Olsson, M. H.; Sondergaard, C. R.; Rostkowski, M.; Jensen, J. H. PROPKA3: Consistent treatment of internal and surface residues in empirical pKa predictions. *J. Chem. Theory Comput.* **2011**, *7* (2), 525−37.

(36) Gautier, R.; Douguet, D.; Antonny, B.; Drin, G. HELIQUEST: a web server to screen sequences with specific alpha-helical properties. *Bioinformatics* **2008**, *24* (18), 2101−2.

(37) Eisenberg, D.; Weiss, R. M.; Terwilliger, T. C. The helical hydrophobic moment: a measure of the amphiphilicity of a helix. *Nature* **1982**, *299* (5881), 371−4.

(38) Nosé, S. A unified formulation of the constant temperature molecular dynamics methods. *J. Chem. Phys.* **1984**, *81* (1), 511−519.

(39) Hoover, W. G. Canonical dynamics: Equilibrium phase-space distributions. *Phys. Rev. A: At., Mol., Opt. Phys.* **1985**, *31* (3), 1695−1697.

(40) Parrinello, M.; Rahman, A. Polymorphic transitions in single crystals: A new molecular dynamics method. *J. Appl. Phys.* **1981**, *52* (12), 7182−7190.

(41) Hess, B.; Bekker, H.; Berendsen, H. J. C.; Fraaije, J. G. E. M. LINCS: A linear constraint solver for molecular simulations. *J. Comput. Chem.* **1997**, *18* (12), 1463−1472.

(42) Hess, B. P-LINCS: A Parallel linear constraint solver for molecular simulation. *J. Chem. Theory Comput.* **2008**, *4* (1), 116−122.

(43) Darden, T.; York, D.; Pedersen, L. Particle mesh Ewald: An N· log(N) method for Ewald sums in large systems. *J. Chem. Phys.* **1993**, *98* (12), 10089−10092.

(44) Jo, S.; Kim, T.; Iyer, V. G.; Im, W. CHARMM-GUI: a web-based graphical user interface for CHARMM. *J. Comput. Chem.* **2008**, *29* (11), 1859−65.

(45) Jo, S.; Lim, J. B.; Klauda, J. B.; Im, W. CHARMM-GUI Membrane Builder for mixed bilayers and its application to yeast membranes. *Biophys. J.* **2009**, *97* (1), 50−8.

(46) Wu, E. L.; Cheng, X.; Jo, S.; Rui, H.; Song, K. C.; Davila-Contreras, E. M.; Qi, Y.; Lee, J.; Monje-Galvan, V.; Venable, R. M.; Klauda, J. B.; Im, W. CHARMM-GUI Membrane Builder toward realistic biological membrane simulations. *J. Comput. Chem.* **2014**, *35* (27), 1997−2004.

(47) Abraham, M. J.; Murtola, T.; Schulz, R.; Páll, S.; Smith, J. C.; Hess, B.; Lindahl, E. GROMACS: High performance molecular

simulations through multi-level parallelism from laptops to super-computers. *SoftwareX* **2015**, *1−2*, 19−25.

(48) Huang, J.; MacKerell, A. D., Jr. CHARMM36 all-atom additive protein force field: validation based on comparison to NMR data. *J. Comput. Chem.* **2013**, *34* (25), 2135−45.

(49) Klauda, J. B.; Venable, R. M.; Freites, J. A.; O'Connor, J. W.; Tobias, D. J.; Mondragon-Ramirez, C.; Vorobyov, I.; MacKerell, A. D., Jr.; Pastor, R. W. Update of the CHARMM all-atom additive force field for lipids: validation on six lipid types. *J. Phys. Chem. B* **2010**, *114* (23), 7830−43.

(50) Jorgensen, W. L.; Chandrasekhar, J.; Madura, J. D.; Impey, R. W.; Klein, M. L. Comparison of simple potential functions for simulating liquid water. *J. Chem. Phys.* **1983**, *79* (2), 926−935.

(51) Humphrey, W.; Dalke, A.; Schulten, K. VMD: visual molecular dynamics. *J. Mol. Graphics* **1996**, *14* (1), 33−38.

(52) Zhuang, X.; Makover, J.; Im, W.; Klauda, J. A systematic molecular dynamics simulation study of temperature dependent bilayer structural properties. *Biochim. Biophys. Acta, Biomembr.* **2014**, *1838*, 2520−29.

(53) Frishman, D.; Argos, P. Knowledge-based protein secondary structure assignment. *Proteins: Struct., Funct., Genet.* **1995**, *23* (4), 566−79.

(54) Cui, H.; Lyman, E.; Voth, G. A. Mechanism of membrane curvature sensing by amphipathic helix containing proteins. *Biophys. J.* **2011**, *100* (5), 1271−9.

(55) Prevost, C.; Sharp, M. E.; Kory, N.; Lin, Q.; Voth, G. A.; Farese, R. V., Jr.; Walther, T. C. Mechanism and Determinants of Amphipathic Helix-Containing Protein Targeting to Lipid Droplets. *Dev. Cell* **2018**, *44* (1), 73−86.

(56) Egashira, M.; Gorbenko, G.; Tanaka, M.; Saito, H.; Molotkovsky, J.; Nakano, M.; Handa, T. Cholesterol modulates interaction between an amphipathic class A peptide, Ac-18A-NH2, and phosphatidylcholine bilayers. *Biochemistry* **2002**, *41*, 4165−4172.

(57) Ladokhin, A. S. Analysis of protein and peptide penetration into membranes by depth-dependent fluorescence quenching: theoretical considerations. *Biophys. J.* **1999**, *76* (2), 946−55.

(58) Paulino, J.; Pang, X.; Hung, I.; Zhou, H. X.; Cross, T. A. Influenza A M2 Channel Clustering at High Protein/Lipid Ratios: Viral Budding Implications. *Biophys. J.* **2019**, *116* (6), 1075−1084.

(59) Glaser, R. W.; Sachse, C.; Durr, U. H.; Wadhwani, P.; Afonin, S.; Strandberg, E.; Ulrich, A. S. Concentration-dependent realignment of the antimicrobial peptide PGLa in lipid membranes observed by solid-state 19F-NMR. *Biophys. J.* **2005**, *88* (5), 3392−7.

(60) Leeb, F.; Maibaum, L. Spatially resolving the condensing effect of cholesterol in lipid bilayers. *Biophys. J.* **2018**, *115* (11), 2179−88.

(61) Pan, J.; Dalzini, A.; Song, L. Cholesterol and phosphatidyle-thanolamine lipids exert opposite effects on membrane modulations caused by the M2 amphipathic helix. *Biochim. Biophys. Acta, Biomembr.* **2019**, *1861* (1), 201−209.

(62) Dobereiner, H. G.; Kas, J.; Noppl, D.; Sprenger, I.; Sackmann, E. Budding and fission of vesicles. *Biophys. J.* **1993**, *65* (4), 1396−1403.

(63) Sackmann, E.; Feder, T. Budding, fission and domain formation in mixed lipid vesicles induced by lateral phase separation and macromolecular condensation. *Mol. Membr. Biol.* **1995**, *12* (1), 21−28.

(64) Lipowsky, R. Domain-induced budding of fluid membranes. *Biophys. J.* **1993**, *64* (4), 1133−1138.

(65) Heberle, F. A.; Feigenson, G. W. Phase separation in lipid membranes. *Cold Spring Harbor Perspect. Biol.* **2011**, *3* (4), a004630.